Geomechanics and Engineering, *Vol. 22, No. 5 (2020) 461-473*
DOI: https://doi.org/10.12989/gae.2020.22.5.461

Strength characteristics and fracture evolution of rock with different shapes inclusions based on particle flow code

Zhi G. Xia[1a], Shao J. Chen[*1], Xing Z. Liu[2b] and Run Sun[3c]

[1]State Key Laboratory of Mine Disaster Prevention and Control, Shandong University of Science and Technology, Qingdao, 266590, China
[2]School of Civil Engineering, Ludong University, Yantai, 264025, China
[3]Yantai Institute of Metrology, Yantai, 264025, China

(Received June 11, 2020, Revised July 29, 2020, Accepted August 4, 2020)

Abstract. Natural rock mass contains defects of different shapes, usually filled with inclusions such as clay or gravel. The presence of inclusions affects the failure characteristics and mechanical properties of rock mass. In this study, the strength and failure characteristics of rock with inclusions were studied using the particle flow code under uniaxial compression. The results show that the presence of inclusions not only improves the mechanical properties of rock with defects but also increases the bearing capacity of rock. Circular inclusion has the most obvious effect on improving model strength. The inclusions affect the stress distribution, development of initial crack, change in crack propagation characteristics, and failure mode of rock. In defect models, concentration area of the maximum tensile stress is generated at the top and bottom of defect, and the maximum compressive stress is distributed on the left and right sides of defect. In filled models, the tensile stress and compressive stress are uniformly distributed. Failing mode of defect models is mainly tensile failure, while that of filled models is mainly shear failure.

Keywords: inclusions; different shapes; strength characteristics; fracture evolution; numerical simulation

1. Introduction

Rock mass is a medium with complex engineering properties, and its interior usually contains holes with different shapes, weak interlayer, and other defects, severely affecting the strength and failure characteristics of rock (Irwin 1957, Wang *et al.* 2020, Wu *et al.* 2020). Fissures and holes in natural rock mass are usually filled with broken rock or clay (Zhao *et al.* 2020, Feng *et al.* 2019). These particles and clay also affect the mechanical properties of rocks to different extents (Wu *et al.* 2020, Xu *et al.* 2020). Furthermore, fissures and holes are often artificially filled to improve the strength of rock mass and reduce the risk of failure of rock mass in actual rock engineering. The presence of inclusions affects the mechanical response and failure characteristics of rock (Griffith 1920, Sammis and Ashby 1986, Carter *et al.* 2010, Katcoff and Graham-Brady 2014). Therefore, it is of great practical significance to study the strength characteristics and fracture evolution of rock containing inclusions.

The internal defects of rock have been extensively investigated, and many meaningful results were obtained (Lee and Hong 2018, Sammis 1986, Hadi *et al.* 2015, Gratchev 2016, Wu and Wang 2020). Taking gypsum as the rock model material, Bobet and Einstein (1998) conducted uniaxial and biaxial compression tests on samples containing two preexisting fissures and studied the fracture coalescence behavior of brittle materials. Morgan and Einstein (2017) conducted a series of unconfined compression tests on prismatic shale specimens with two preexisting flaws and various bedding plane orientations. As the bedding planes became more aligned with the direction of maximum compressive stress, the cracks initiating at the flaw tips propagated more frequently along them. Wong and Lin (2015) used a numerical simulation software RFPA3D to study the crack propagation and stress changes in heterogeneous rocks with multiple holes and proposed an accurate crack coalescence criterion. Gratchev *et al.* (2016) studied the effects of length and width of a flaw on the strength of rock-like specimens. The specimens with longer and wider flaws had lower strength, and failure was mainly caused by a shear crack.

The effect of inclusions on the mechanical properties of defective rock is relatively complex. At present, the effect of inclusions on rock properties has attracted much attention (Maji and Shah 1989, Komurlu *et al.* 2016). Tasdemir *et al.* (1989) studied variations in the peak strength of concrete specimens containing single filled fissures with different incline angles. Miao *et al.* (2018) studied the damage and fracture evolution of rock with a single fissure under four filling conditions of no filling, gypsum filling, cement filling, and resin filling and believed that the sample after filling had a higher crack initiation stress level and a smaller crack dip angle. Maji and Shah (1989) first performed experiments on prismatic concrete specimens containing two circular inclusions and unfilled holes. Matrix cracking was always initiated at the top and bottom of holes, while

∗Corresponding author, Ph.D.
E-mail: kd_duanceng@163.com

http://www.techno-press.org/?journal=gae&subpage=7
ISSN: 2005-307X (Print), 2092-6219 (Online)

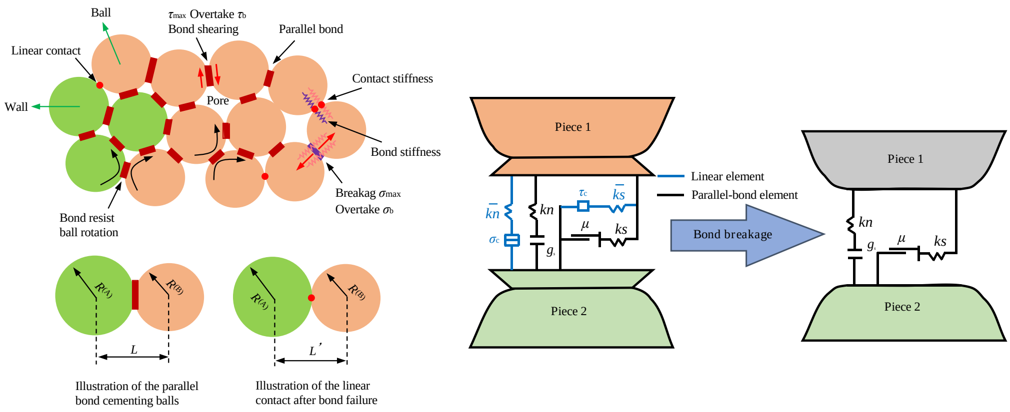

Fig. 1 Parallel bond model

interface cracking initiated at the inclusion interface. Zhu *et al.* (2019) studied the effect of inclusions in a hole on the mechanical properties and fracture evolution of rock; the type and shape of inclusions were considered as important factors affecting the strength and deformation characteristics of sandstone. Janeiro *et al.* (2010) conducted uniaxial compression tests on gypsum samples containing one or two inclusions with different strengths, stiffness, shapes, and sizes and analyzed the crack coalescence of samples with inclusions.

An actual rock mass contains defects of various shapes. However, the mechanical response and crack propagation of these defective rock masses are still unclear, and the interaction between defective rock masses and defects of different shapes is still unclear. Moreover, defects with different shapes filled with inclusions have been rarely studied. Therefore, the effect of inclusions on the failure and stress evolution of defective rock should be studied further. Therefore, a two-dimensional (2D) particle flow code (PFC) was used to study the strength characteristics and fracture evolution of defective rocks with different shapes of inclusions, and the stress distribution characteristics before crack formation and after model failure were also analyzed.

2. Methodology

2.1 PFC

Particle flow theory was created by Cundall and Strack (1979) on the basis of discrete element method. Rigid particles and bonds are usually used to characterize the rock materials in PFC. Rigid particles are represented by disks with a unit thickness in PFC2D or by balls in three-dimensional (3D) PFC, and these particles can both translate and rotate. The force and displacement between particles are achieved through bonds. There are two types of bond, namely, contact bond (CB) and parallel bond (PB), which can be used to simulate the connection between rock particles, as shown in Fig. 1 (Cho *et al.* 2007, Lisjak and Grasselli 2014). The CB has slight resistance to moment caused by particle rotation or shear, while the PB not only transfers force but also transfers moment. In Fig. 1, k_n and k_s are particle contact stiffness, and Pb-k_n and Pb-k_s are bonding stiffness. When the bond is broken, the forces and moments transferred by parallel bonds disappear, and the bonding stiffness loses its effect. However, as long as the particles remain in contact, the contact stiffness is still effective. The PBM model in PFC can well simulate the mechanical and failure characteristics of rock (Wang *et al.* 2020, Wen *et al.* 2017). In this study, the parallel bond model was used to characterize rock.

2.2 Acoustic emission simulation in PFC

Bonding strength can directly reflect the macro strength of rock in numerical models. If the stress transferred between particles exceeds the bonding strength between the particles, the bonds between the particles will break, and microcracks will appear in the rock samples (Hazzard *et al.* 2000). When microcracks propagate in rock, the damage energy is rapidly released in the form of acoustic waves, known as the acoustic emission phenomenon (Wen *et al.* 2017). Therefore, during numerical experiments, acoustic emission events can be simulated by calculating the number of bond break of particles. Because of the limitation of calculation ability, it is difficult to determine the response of macro rock from the particle size and number in PFC2D, but the mechanical laws reflected in PFC2D are helpful to understand the acoustic emission of rock.

2.3 Determination of microscopic parameters

Microscopic parameters of particles are very important in the numerical simulation of PFC2D. However, these microscopic parameters cannot be directly obtained from laboratory tests. Therefore, it is necessary to determine the microscopic parameters so that the numerical simulation results are consistent with the laboratory test results. First, the basic mechanical parameters of rock are obtained by conducting a large number of laboratory tests. Then, numerical simulations with different microscopic parameters are carried out to calculate the mechanical parameters of rock. The microscopic parameters should be checked constantly until the microscopic parameters can make the numerical results consistent with the laboratory test results. The determination of microscopic parameters in

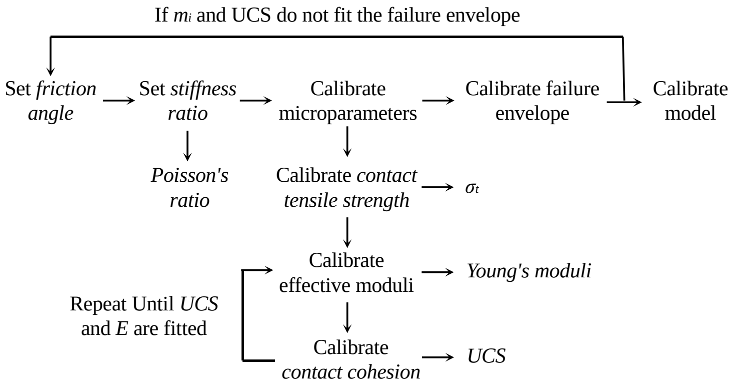

Fig. 2 Calibration procedure of microscopic parameters (Castro-Filgueira *et al.* 2017)

Table 1 Microscopic parameters of rock and inclusion

Rock		Inclusion	
Parameter	Value	Parameter	Value
Minimum particle diameter (mm)	0.3	Minimum particle diameter (mm)	0.3
Particle diameter ratio	1.5	Particle diameter ratio	1.5
Density (kg/m^3)	2490	Density (kg/m^3)	1600
Contact modulus of the particle (GPa)	3.19	Contact modulus of the particle (GPa)	1.62
Contact bond gap (mm)	0.05	Contact bond gap (mm)	0.05
Porosity	0.1	Porosity	0.1
Parallel bond friction angle (°)	32	Parallel bond friction angle (°)	29
Parallel bond tensile strength (MPa)	22.3	Parallel bond tensile strength (MPa)	2.27
Normal critical damping ratio	0.5	Normal critical damping ratio	0.5
Parallel bond cohesive force (MPa)	32.3	Parallel bond cohesive force (MPa)	4.92

PFC2D is shown in Fig. 2. The parameter of m_i is Hoek-Brown strength parameter (Hoek and Brown 1980).

In this paper, the microscopic parameters of rock and inclusion are shown in Table 1. The calibration results of microscopic parameters of rock and inclusion are shown in Fig. 3. The peak strength and elastic modulus of test sample and numerical sample are the same. Although the peak strains of two samples are different, they are both within the acceptable range.

2.4 Model design

To study the mechanical response and crack propagation of defective rocks with different shapes of inclusion, six geometric shapes of defect were established, including eight models. Among them, the triangular model had an equilateral triangle and a 90° counterclockwise rotation triangle, and the square model had a square and a 45° counterclockwise rotation square. The height of rock model was 100 mm, and the width was 50 mm. The defect was set at the center of specimen. The defect areas of all shapes were the same, about 79.2 mm^2. The sizes of rock model and defect are shown in Fig. 4(a) and Table 2. Furthermore, the defects were filled with inclusion in this study. The defect model and filled model are shown in Fig. 4(b).

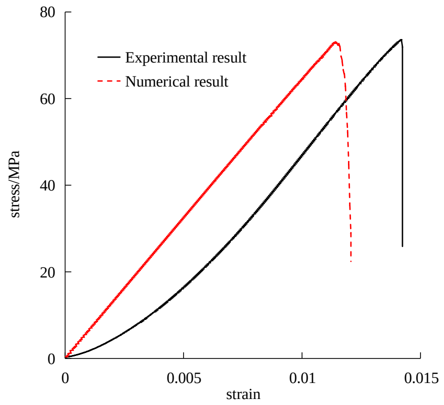

(a) Parameter calibration of rock

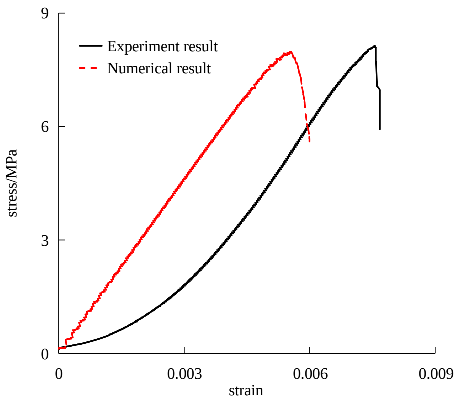

(b) Parameter calibration of inclusion

Fig. 3 Calibration results of microscopic parameters

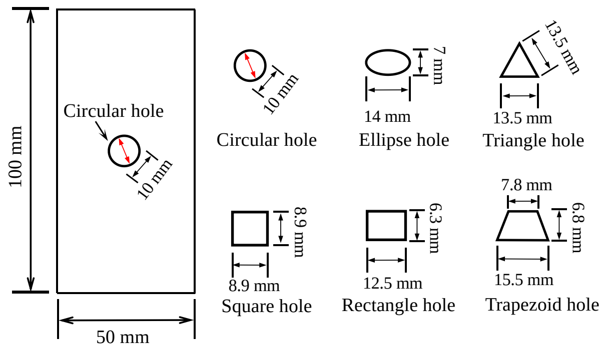

(a) Schematic diagram of numerical model

Fig. 4 Numerical model

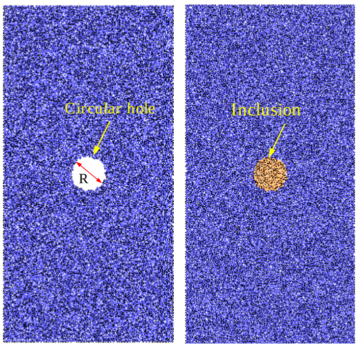

(b) Defect model and filled model

Fig. 4 Continued

Table 2 Geometric parameters of defect holes

Species	Circular	Elliptical	Triangular	Square	Rectangular	Trapezoidal
Area (mm^2)	78.54	76.97	78.91	79.21	78.75	79.22
Error %	0.86%	2.84%	0.39%	0.01%	0.59%	0.0%
Size (mm)	10	14 and 7	13.5	8.9	12.5 and 6.3	15.5, 8 and 6.8

The error is the comparison of area of each defect with the trapezoidal defect. The size (mm) of each hole is shown in Fig. 4(a).

3. Analyses of numerical simulation results

3.1 Mechanical properties of defect models and filled models

Stress-strain curve and crack number-strain curve of defect models and filled models are shown in Fig. 5. The stress-strain curve of the same shape defect model is consistent with the corresponding crack-strain curve. The stress-strain curve and crack-strain curve of rock with different defect holes and filled holes have almost the same trend. However, the stress-strain curve of filling model significantly fluctuates near the peak value and has a sawtooth shape, mainly because of a rapid propagation of crack releases the stress and the difference in the secondary crack propagation characteristics of filled rock samples with different shapes. Fig. 5 shows that the stress-strain curves of each model have no initial compaction stage compared with laboratory test results. This is mainly because the particles in PFC are rigid, and there is no initial damage in the model. From the curve after the peak stress, it can be observed that the failure mode of selected defect model material is brittle, and the failure of rock is still brittle after filled.

The crack number-strain curves in Fig. 5 show that the crack development of defect models and filled models has three stages: no crack stage, slow crack growth stage, and fast crack growth stage. In the initial loading stage, because the stress level is low, no crack propagation occurs in the sample. As the load increases, cracks appear gradually. Before approaching the peak strength, cracks grow slowly, and a large number of cracks appear after reaching the peak strength.

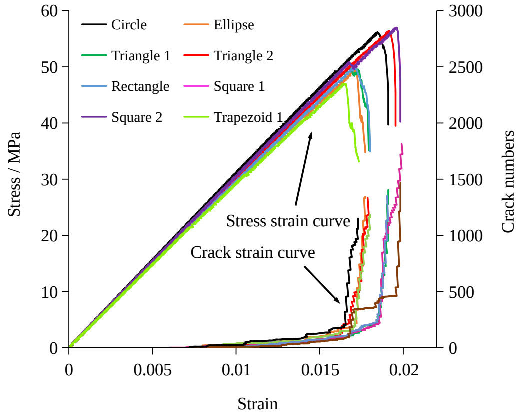

(a) Defect models

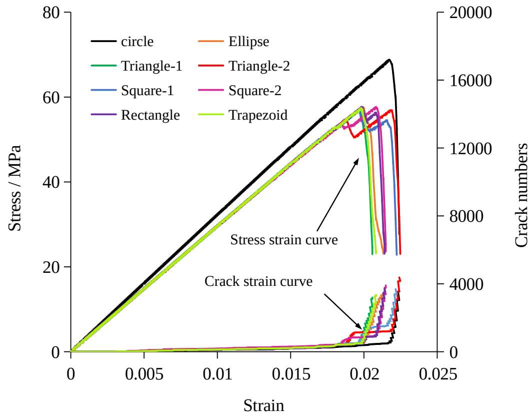

(b) Filled models

Fig. 5 Stress-strain curve and crack number-strain curve

Fig. 6 shows comparison curves of peak stress, peak strain, elastic modulus, and crack numbers between defect models and filled models, and the specific values are shown in Table 2. As shown in Fig. 6(a), the peak stress of defect models and filled models is less than that of intact rock, the peak stress of filled model is greater than that of defect model, and the peak stress of circular filled model is greater than that of other defect filled models. Except for the circular filled model, the peak stress of other filled models is the same. Fig. 6(b) shows that the peak strains of defect models and filled models are both larger than that of intact rock, and the peak strain of filled model is larger than that of defect model. Fig. 6(c) shows the elastic modulus of defect models and filled models. The elastic modulus of defect model and filled model is less than that of intact rock, and the elastic modulus of filled model is larger than that of defect model. The total number of cracks obtained after the failure of filled model is larger than that of defect model shown in Fig. 6(d). This is because the bearing capacity of filled rock sample is significantly improved, and more energy is accumulated before failure under uniaxial compression. Therefore, the energy release rate during the final failure is larger, further leading to the aggravation failure of rock sample. Because of the effect of defects, the bearing capacity of samples is significantly deteriorated compared to the intact rock samples. The peak strength, peak strain, and elastic modulus of models with inclusions

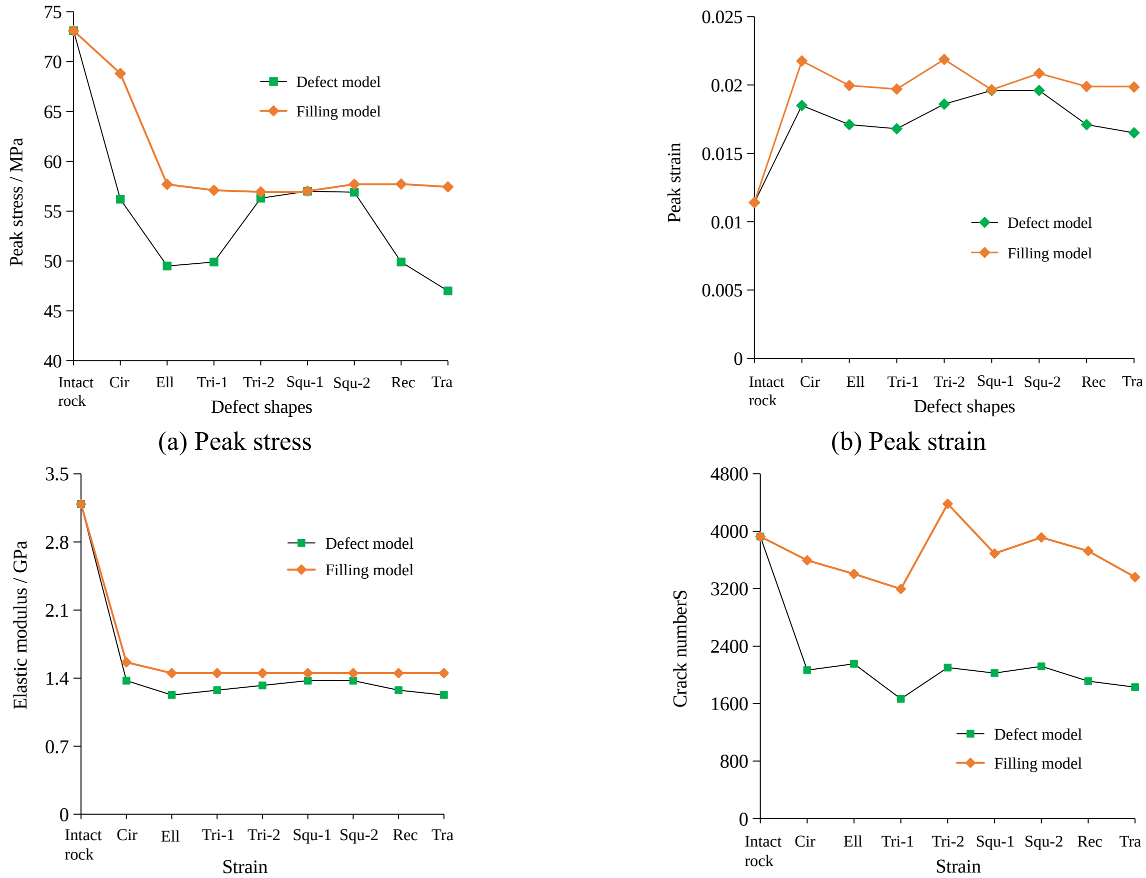

(a) Peak stress (b) Peak strain

(c) Elastic modulus (d) Crack numbers

Fig. 6 Comparison of mechanical parameter curves and crack number curve between defect models and filled models

Table 3 Mechanical parameters and crack numbers of defect model and filled model under uniaxial compression

Category	Defect Models				Filled Models			
	Peak stress (MPa)	Peak strain	*E* (GPa)	Crack numbers	Peak stress (MPa)	Peak strain	*E* (GPa)	Crack numbers
Circle hole	56.2	0.0185	1.374	2066	68.8	0.0217	1.563	3595
Ellipse hole	49.5	0.0171	1.226	2154	57.69	0.0200	1.451	3406
Triangle hole-1	49.9	0.0168	1.276	1666	57.10	0.0197	1.451	3196
Triangle hole-2	55.3	0.0186	1.325	2102	56.9	0.0218	1.451	4382
Square hole-1	57.0	0.0196	1.374	2025	57.01	0.0196	1.451	3690
Square hole-2	56.9	0.0196	1.374	2119	57.70	0.0208	1.451	3914
Rectangle hole	49.9	0.0171	1.276	1913	57.72	0.0199	1.451	3725
Trapezoid hole	47.0	0.0165	1.226	1829	57.44	0.0199	1.451	3361

of different shapes are slightly different and mostly the same. Therefore, inclusion plays a very good supporting role for the model and improves the peak strength, peak strain, and elastic modulus. Among them, the peak strength of circular filled model increased the most, about 22.4%, and the peak strength of square-1 filled model increased the least, because the stress state inside the rock samples is significantly influenced by the shapes of inclusions. The peak strain of trapezoidal filled model increased the most, about 20.6%, and the peak strain of square-1 filled model did no change. The elastic modulus of elliptical and trapezoidal filled models increased the most, about 18.35%, and the elastic modulus of square-1 and square-2 models increased the least, about 5.6%. Different shapes of inclusions have different effects on rock strength and crack numbers, requiring further study and investigation.

3.2 Failure characteristics of defect models and filled models

Fig. 7 shows the parallel bond force diagram of defect models and filled models before and after model failure. The red force chains represent tensile force, and the black force chains represent compression force in Fig. 7.

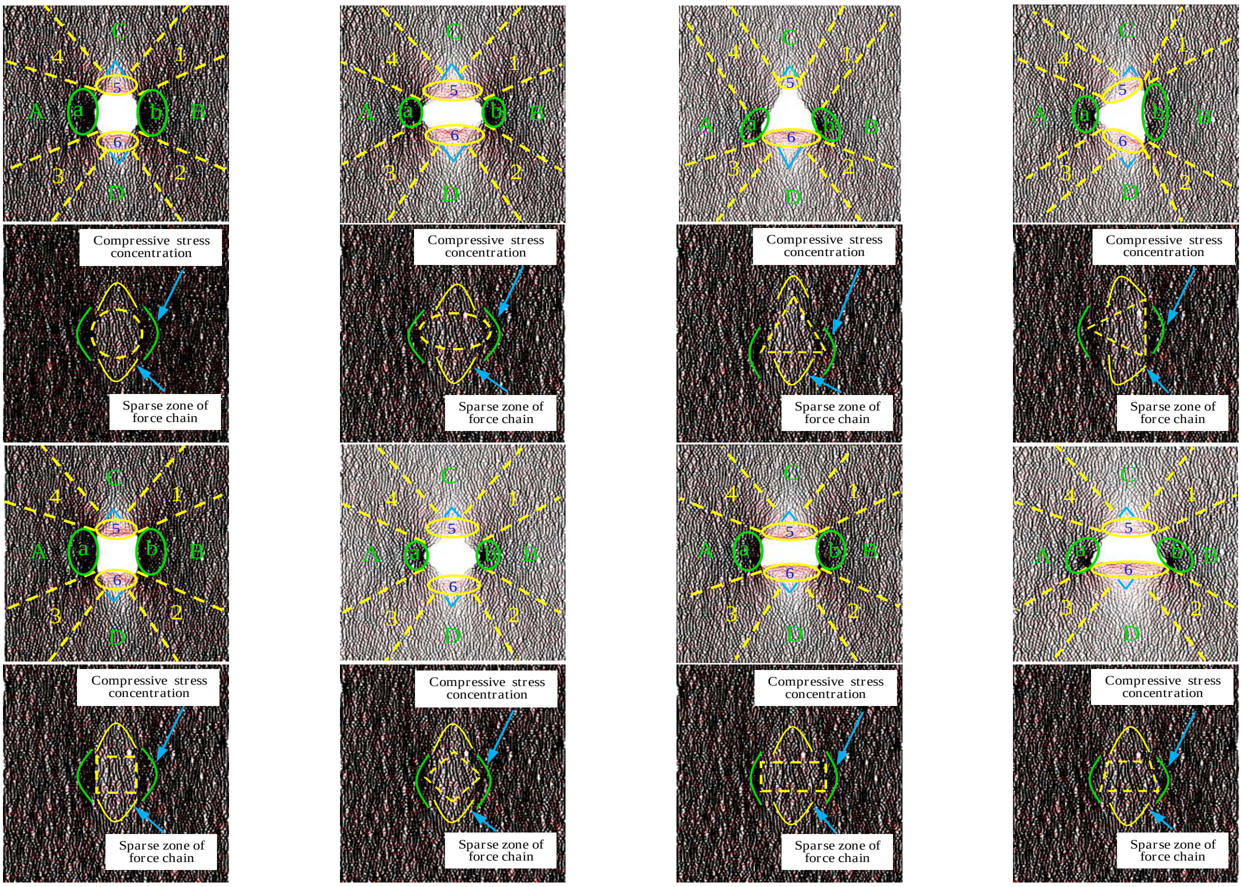

(a) Parallel bond force diagram of defect models and filled models before model failure

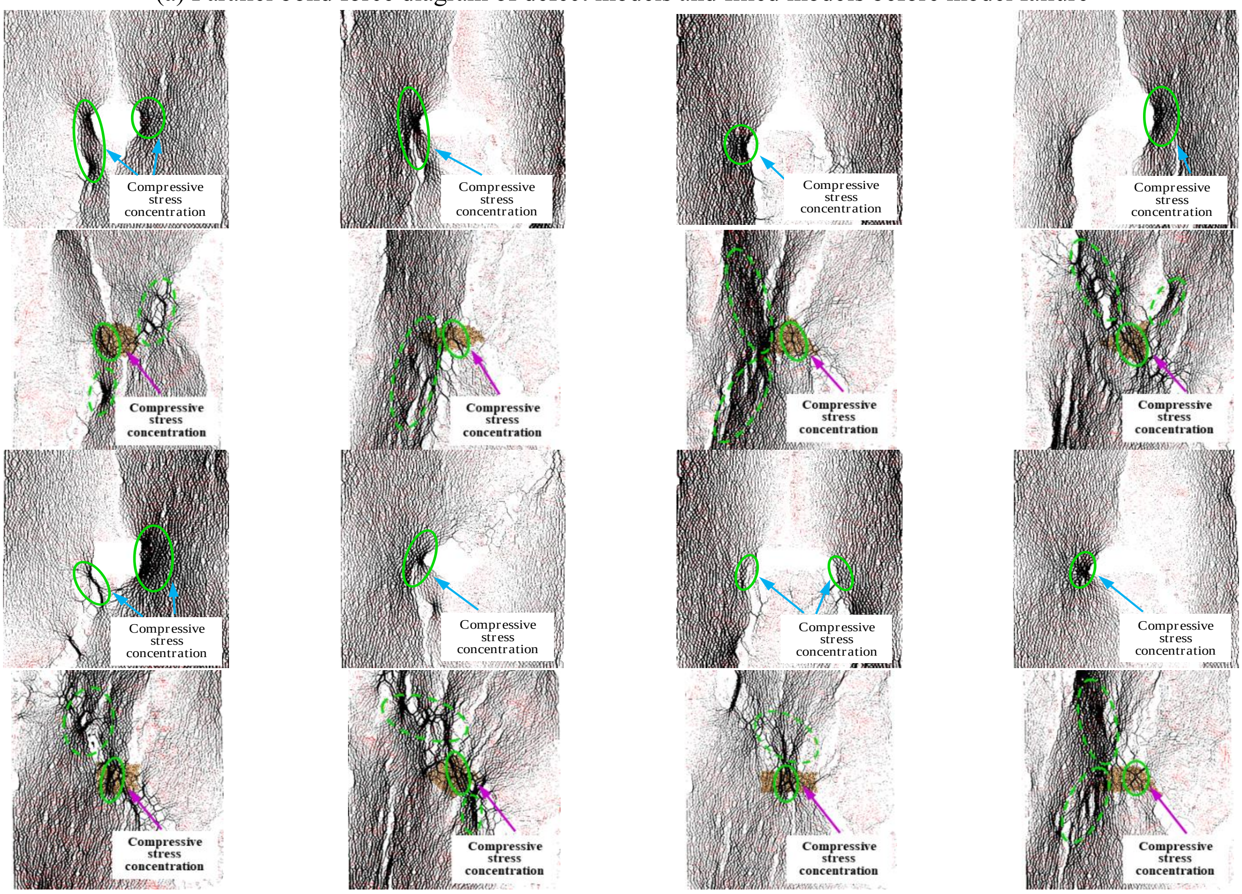

(b) Parallel bond force diagram of defect models and filled models after model failure

Fig. 7 Parallel bond force diagram of defect models and filled models before and after model failure

Furthermore, the denser the force chains are in the parallel bond force diagram, the darker the color shown in Fig. 7 and the larger the stress. Fig. 7(a) shows that before crack formation, the tensile stress of defect model is distributed around the defect in a butterfly shape (areas 1, 2, 3, and 4), and the maximum tensile stress is generated at the top and bottom of defect (areas 5 and 6). The compressive stress is widely distributed in the whole model (areas A, B, C, and D), and the maximum compressive stress occurs on the left and right sides of defect (areas a and b). The tensile stress and compressive stress are uniformly distributed in filled models. However, the force chains around defect are sparse than those in other areas, indicating that the bearing capacity of inclusion is weaker than that in other areas. By comparing the parallel bond force diagram between defect models and filled models, it was found that the force chains are denser in filled models, and the bearing capacity of filled model is significantly greater than that of defect model before the crack occurs. Fig. 7(b) shows that the compressive stress in defect models is also distributed on the left or right side of defect after model failure, while the compressive stress in filled models is distributed across inclusions. The compressive stress concentration range in filled models is obviously larger than that in defect models.

The final failure diagrams of defect models and filled models are shown in Fig. 8. Because the bearing capacity is improved by inclusions, the damage degree of filled model is obviously greater than that of defect model. By comparing the failure diagrams of defect models and filled models, it was found that the crack distributions and model failure characteristics of the two types of model samples are different. In filled models, the main failure surface penetrates the entire rock sample diagonally. However, in defect models, in addition to the fractures along the diagonal of model, tensile fractures are formed at the top or bottom of defect. This is because under uniaxial compression, tensile stress is generated at these positions inside the rock sample. As it is well known that the initial crack may induce the propagation of other cracks, changing the subsequent crack propagation characteristics, the final failure modes of rock sample are different. Therefore, crack propagation should be studied to explain the effect of inclusion shapes on rock failure characteristics.

3.3 Crack propagation and stress evolution

Crack propagation and stress evolution of square defect model and square filled model are shown in Fig. 9. Stress-strain and acoustic emission-strain diagrams of square defect model and square filled model are shown in Fig. 10. In the defect model, tensile stress concentration areas are generated at the top and bottom of defect, and compressive stress concentration areas are generated on the left and right sides of defect before crack formation. The maximum compressive stress is 44 MPa, and the maximum tensile stress is 2 MPa. Owing to the low stress level, the defect does not achieve tensile strength and compressive strength around the defect, and the sample does not have crack propagation. Therefore, almost no acoustic emission phenomenon was observed. The acoustic emission at this time corresponds to point a in Fig. 10(a). Because the tensile strength of rock is less than the compressive strength of rock, tensile fractures initially appear at the top and bottom of defect. Sporadic acoustic emission events occur at this time, as shown by point b in Fig. 10(a). As the load increases, far-field cracks and local internal cracks are gradually generated at the end and inside the model. Cracks begin to gather diagonally along the sample due to compressive stress concentration in these areas. Acoustic emission is relatively obvious at these stages, corresponding to points c and d in Fig. 10(a). As the loading continues, a large number of cracks are generated along the diagonal of model. The model is finally destroyed diagonally along the sample with the generation of a large number of cracks. At this time, the acoustic emission corresponds to point e in Fig. 10(a).

In the filled model, there is no tensile stress, and the maximum compressive stress is about 2 MPa near the filled area before the crack is generated. Similar to the defect model, no crack is generated, and no acoustic emission appears at this time (corresponding to point a in Fig. 10(b)). As the loading progresses, shear failure occurs in inclusion because the strength of inclusion material is lower than that of other areas of model. The following crack propagation, stress concentration area, stress concentration range, and acoustic emission characteristics of filled model are similar to the evolution of defect model. However, the stress-strain curve of filling model significantly fluctuates near the peak value. At this time, the cracks inside the filling body have full growth, and the filling body has yielded and lost its bearing capacity. The complete failure of inclusion decreases the peak value. Because the particles present inside the sample still have a supporting effect at this time, the peak stress appears to increase again. As loading continues, cracks inside the rock mass begin to grow rapidly, and the rock gradually loses the bearing capacity while the cracks continue to increase, causing two more obvious acoustic emission phenomena as shown in Fig. 10 (b).

Because of the effect of defect, the initial crack distribution is different in defect model and filled model. Although the initial crack slightly affects the unstable failure process of rock sample, it induces the propagation of other cracks, thus changing the subsequent crack propagation characteristics. The strain corresponding to feature point a in Fig. 10(b) is smaller than that in Fig. 10(a), i.e., owing to the effect of inclusion, the crack development of filled model occurs earlier than that of defect model, and the acoustic emission phenomenon appears earlier than defect model.

Typical cracking sequences of defect models and filled models with different shapes of defect or inclusion are summarized in Table 3. The crack behaviors of models are mainly divided into two types, i.e., tensile crack and shear crack, labeled with T and S, respectively, in Table 3. A comparison of cracking sequence between the defect model and filled model indicates that the inclusion significantly affects the crack initiation and propagation. In all defect models, tensile cracks first initiate from the top and bottom of defect and propagate parallel to the loading direction.

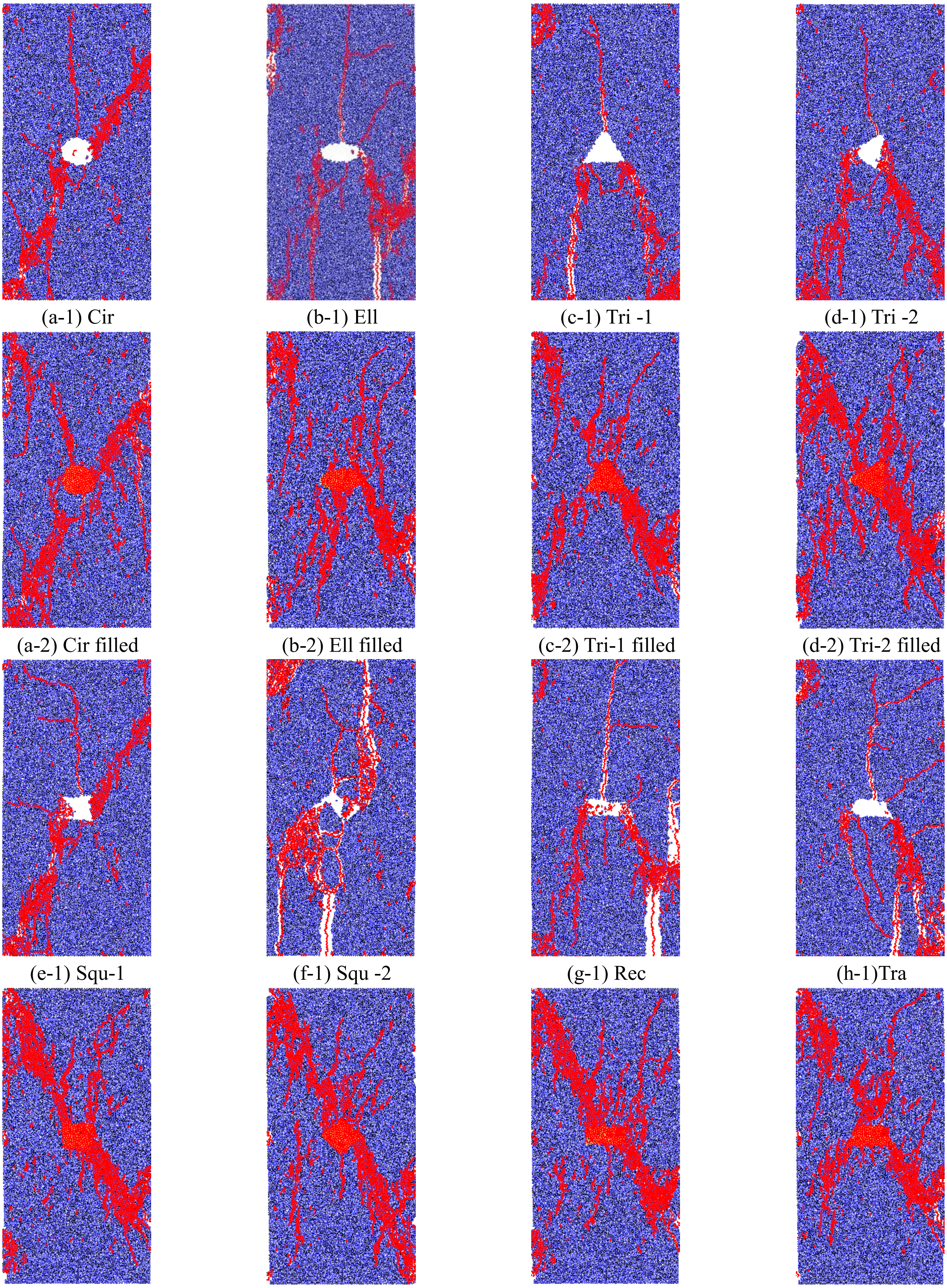

(a-1) Cir (b-1) Ell (c-1) Tri -1 (d-1) Tri -2

(a-2) Cir filled (b-2) Ell filled (c-2) Tri-1 filled (d-2) Tri-2 filled

(e-1) Squ-1 (f-1) Squ -2 (g-1) Rec (h-1)Tra

(e-2) Squ-1filled (f-2) Squ-2 filled (g-2) Rec filled (h-2) Tra filled

Fig. 8 Final failure diagram of defect models and filled models

However, in all filled models, shear cracks are first initiated in inclusion. Then, the cracks penetrate across inclusion and propagate into rock as the load increases. Failing mode of defect models is mainly tensile failure, while that of filled models is mainly shear failure.

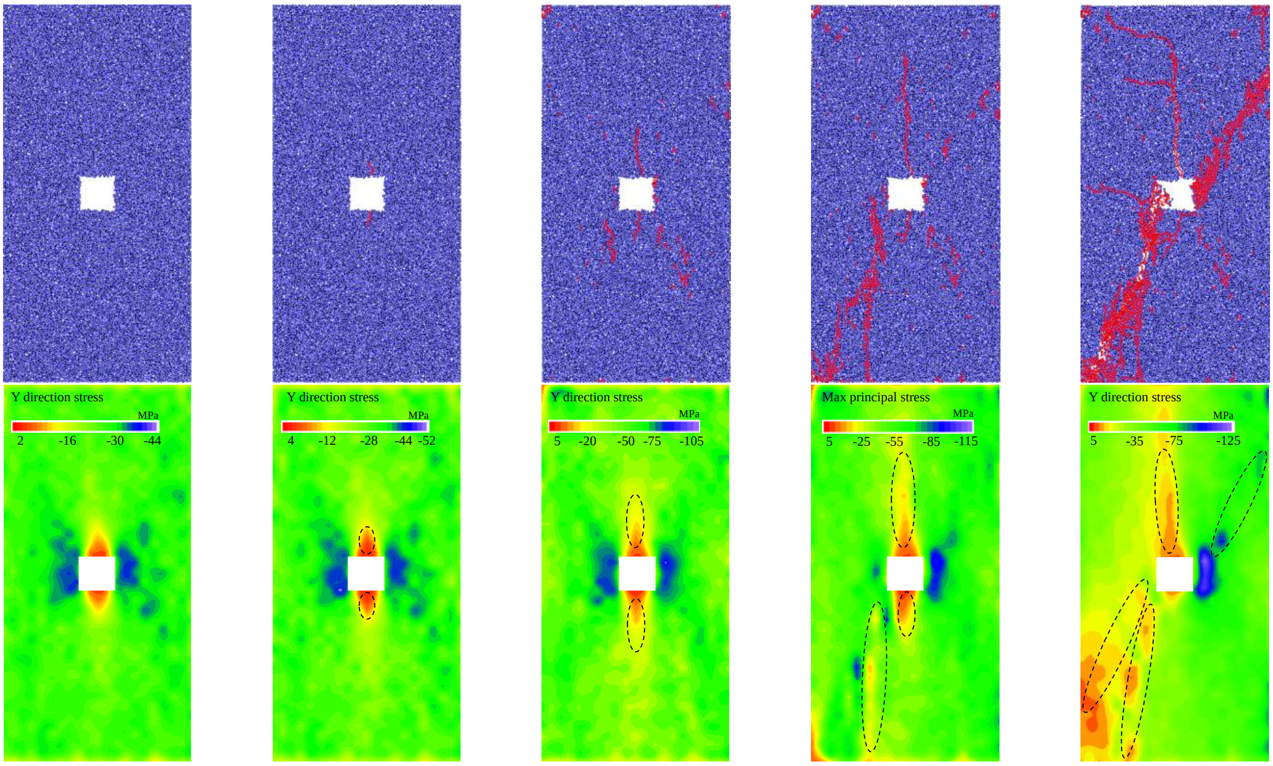

Strain 6.32/10^{-3} Strain 9.67/10^{-3} Strain 18.27/10^{-3} Strain 18.9/10^{-3} Strain 19.09/10^{-3}

(a) Square defect model

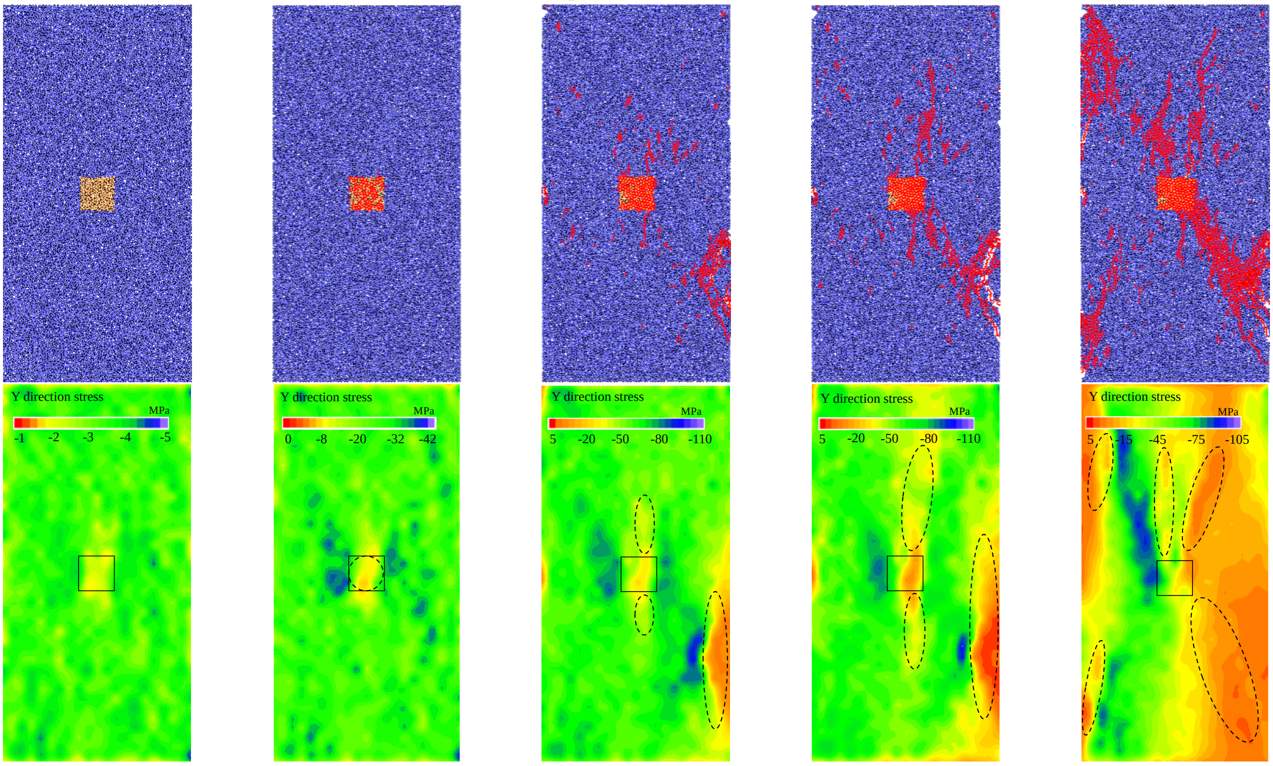

Strain 1.12/10^{-3} Strain 9.94/10^{-3} Strain 19.89/10^{-3} Strain 21.22/10^{-3} Strain 21.67/10^{-3}

(b) Square filled model

Fig. 9 Crack propagation and maximum principal stress evolution of model with square defect (a negative value represents compressive stress, and a positive value represents tensile stress)

The above analysis shows that the initial crack development and stress concentration areas of defective rocks mostly occur at the ends and corners of defects, and the number of vertices of angles of different geometric

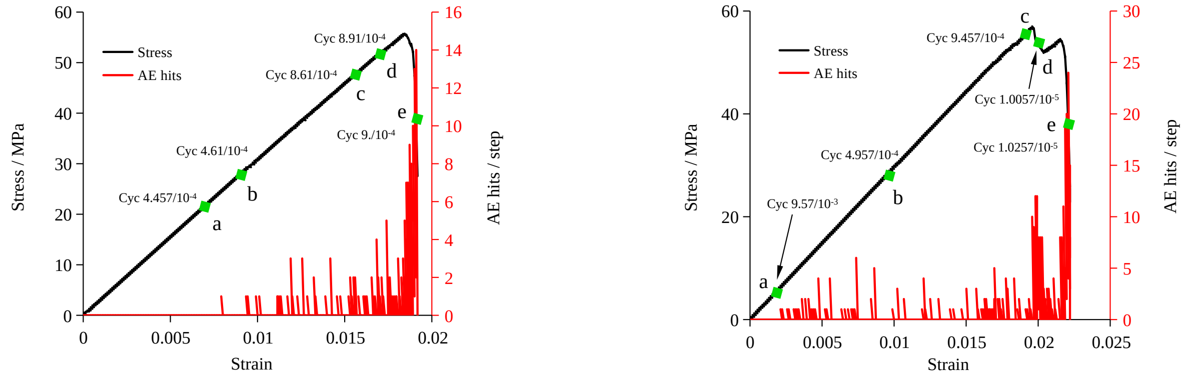

(a) Square defect model (b) Square filled model

Fig. 10 Stress-strain and AE-strain diagram of model with square defect

Table 3 Typical cracking sequences and relative stress levels for each inclusion shape

Defect shape	Filling conditions	Typical cracking sequence and relative stress levels					
Circle	Defect	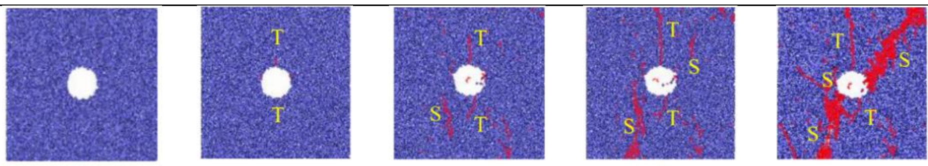	35 %	60.25 %	98.93 %	92.88 %	60 %
	Filled	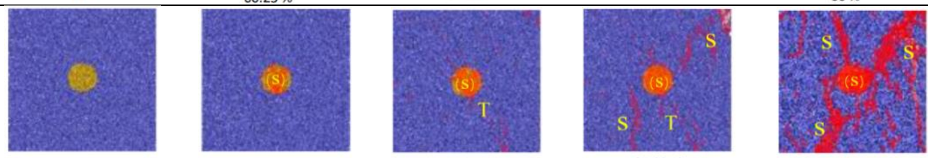	5.06 %	64.04 %	96.8 %	97.02 %	60 %
Ellipse	Defect	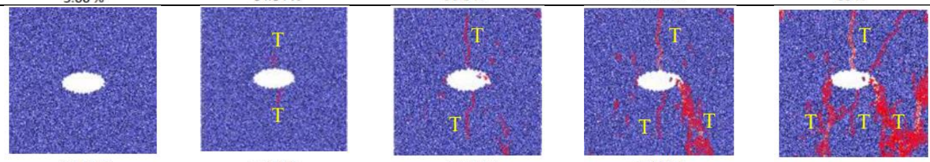	38.18 %	57.92 %	99.19 %	77.98 %	60 %
	Filled	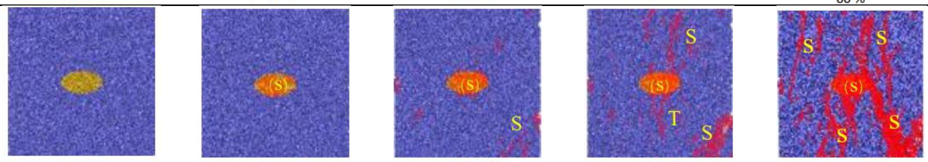	5.89 %	45.41 %	94.63 %	92.55 %	60 %
Triangle-1	Defect	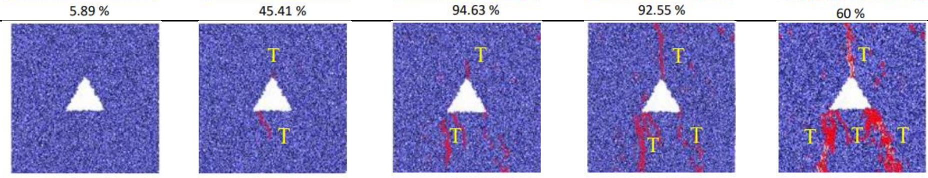	38.68 %	71.34 %	97.79 %	97.0 %	60 %
	Filled	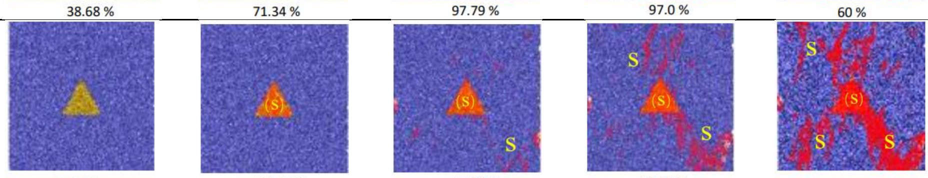	5.88 %	51.49 %	95.44 %	88.09 %	60 %
Triangle-2	Defect	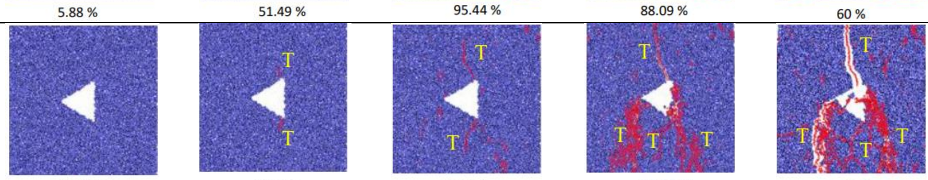	31.97 %	56.66 %	96.80 %	64.12 %	60 %

Table 3 Continued

Defect shape	Filling conditions	Typical cracking sequence and relative stress levels
Triangle-2	Filled	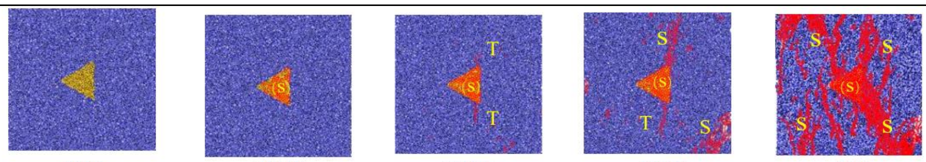 5.88 %, 51.49 %, 95.45 %, 88.09 %, 60 %
Square-1	Defect	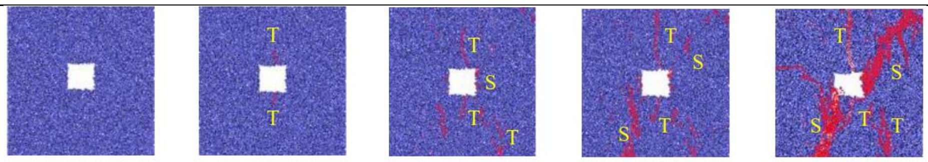 34.38 %, 59.12 %, 96.84 %, 91.58 %, 60 %
	Filled	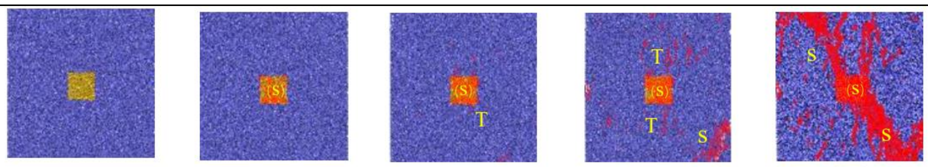 5.89 %, 40.35 %, 85.61 %, 95.26 %, 60 %
Square-2	Defect	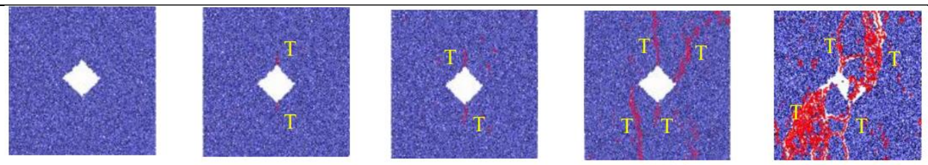 33.92 %, 65.20 %, 87.17 %, 98.42 %, 60 %
	Filled	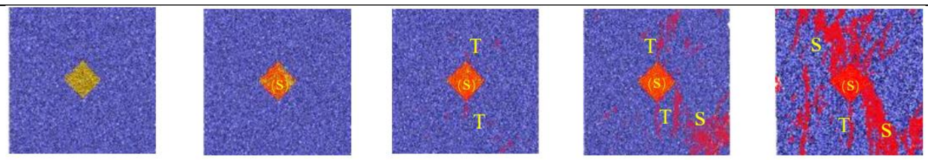 5.82 %, 45.41 %, 83.71 %, 86.14 %, 60 %
Rectangle	Defect	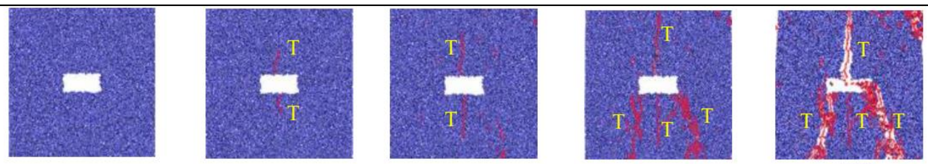 38.07 %, 54.91 %, 95.79 %, 93.18 %, 60 %
	Filled	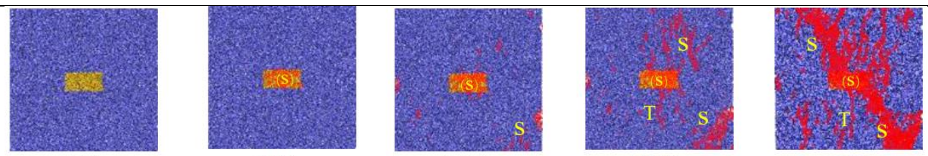 5.82 %, 56.67 %, 96.88 %, 92.2 %, 60 %
Trapezoid	Defect	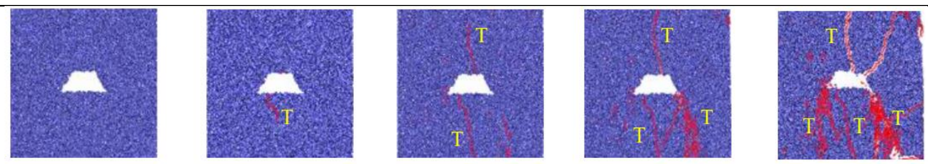 39.78 %, 54.89 %, 95.53 %, 94.04 %, 60 %
	Filled	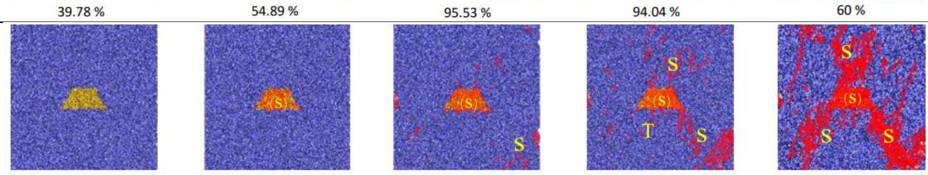 5.85 %, 51.39 %, 95.12 %, 93.9 %, 60 %

shape models is determined from the number of angles. This is also a factor affecting the crack growth and stress distribution of rock. In this study, eight defect models with different geometry shapes were studied. They can be divided into three categories: one angle (Circle hole, Ellipse hole), three angles (Triangle-1 hole, Triangle-2 hole), and four angles (Square-1 hole, Square-2 hole, Rectangle hole, and Trapezoid hole). From the distribution of contact force chains and crack propagation shown in Figs. 7 and 8, it was found that the distribution position and range of tensile stress and compressive stress concentration area of defect model with different number of angles are different, and the crack propagation position and degree are also different. This indicates that the number of angles in the defect rock significantly affects the crack propagation and stress distribution. The compressive stress and tensile stress concentration areas of Circle hole model and Square-1hole model are mainly distributed in the left and right ends and the upper and lower ends of the model, respectively. Because of the number of their angles, the compressive stress and tensile stress concentration regions of Square-1hole model are larger than those of Circle hole model. In the Triangle-1hole model, the compressive stress concentration areas are mainly divided in the bottom two vertices, and the distribution areas are smaller. However, the tensile stress concentration areas are mainly distributed in the bottom, and the tensile stress concentration areas at the upper vertices are smaller. This further shows that the number of angles in the defect model affects the stress distribution of rock. Moreover, in Triangle-1 hole and Triangle-2 hole models, Square-1 hole and Square-2 hole models, although their respective geometries and number of angles are the same, the distribution of stress and crack propagation are also different because of different positions of angle, indicating that the position of angle also significantly affects the crack propagation and stress distribution. Although the crack propagation and stress distribution of each model after filling are different, they are generally consistent. The crack propagation and stress distribution in rock are affected by many factors, not only by the number of angles, but also by the position and direction of the angle. In practical engineering, we should consider the effect of defects or weak interlayer on the distribution of stress field of rock mass from many aspects to improve the safety factor during construction.

4. Conclusions

• Inclusions play a good role in supporting the model and improve the bearing capacity of rock sample. The peak stress and elastic modulus of defect models and filled models are less than those of intact rock, but after filling defects by inclusions, the peak stress, peak strain, and elastic modulus of rock sample increased. Among them, the peak strength of circular filled model increased the most.

• Inclusions affect the distribution of stress in models. In defect models, tensile stress is mainly distributed around the defect in a butterfly shape. The maximum tensile stress concentration area is generated at the top and bottom of defect, and the maximum compressive stress is distributed on the left and right sides of defect. In filled models, the tensile stress and compressive stress are uniformly distributed. However, the force chains around defect are sparse than those in other areas, indicating that the bearing capacity of inclusion is weaker than that in other areas.

• Fracture evolution of rock is influenced by inclusions. In all defect models, tensile cracks are first initiated from the top and bottom of defect and propagate parallel to the loading direction. However, in all filled models, shear cracks are first initiated in inclusion. Then, the cracks penetrate across inclusion and propagate into rock as the load increases. Failing mode of defect models is mainly tensile failure, while that of filled models is mainly shear failure.

Acknowledgments

This study was supported by the National Natural Science Foundation of China (51474134, 51774194), Shandong Provincial Natural Science Fundation for Distinguished Young Scholars (JQ201612), Major basic research projects of Shandong Natural Science Foundation (ZR2018ZC07 40), Taishan Scholar Talent Team Support Plan for Advantaged & Unique Discipline Areas.

References

Bobet, A. and Einstein, H.H. (1998), "Fracture coalescence in rock-type material under uniaxial and biaxial compression", *Int. J. Rock Mech. Min. Sci.*, **35**(7), 863-888. https://doi.org/10.1016/S0148-9062(98)00005-9.

Cao, R.H., Cao, P., Lin, H., Pu, C.Z. and Ou, K. (2016), "Mechanical behavior of brittle rock-like specimens with pre-existing fissures under uniaxial loading: Experimental studies and particle mechanics approach", *Rock Mech. Rock Eng.*, **49**, 763-783. https://doi.org/10.1007/s00603-015-0779-x.

Carter, B.J., Lajtai, E.Z. and Petukhov, A. (2010), "Primary and remote fracture around underground cavities", *Int. J. Numer. Anal. Meth. Geomech.*, **15**, 21-40. https://doi.org/10.1002/nag.1610150103.

Castro-Filgueira, U., Alejano, L.R., Arzúa, J. and Ivars, D.M. (2017), "Sensitivity analysis of the micro-parameters used in a PFC analysis towards the mechanical properties of rocks", *Proc. Eng.*, **191**, 488-495. https://doi.org/10.1016/j.proeng.2017.05.208.

Cho, N., Martin, C.D. and Sego, D.C. (2007), "A clumped particle model for rock", *Int. J. Rock Mech. Min. Sci.*, **44**(7), 97-1010. https://doi.org/10.1016/j.ijrmms.2007.02.002.

Feng, F., Chen, S.J., Li, D.Y., Hu, S.T., Huang, W.P. and Li, B. (2019), "Analysis of fractures of a hard rock specimen via unloading of central hole with different sectional shapes", *Energy Sci. Eng.*, **7**(6), 2265-2286. https://doi.org/10.1002/ese3.432.

Gratchev, I., Dong, H.K. and Chong, K.Y. (2016), "Strength of rock-like specimens with preexisting cracks of different length and width", *Rock Mech. Rock. Eng.*, **49**(11), 4491-4496. https://doi.org/10.1007/s00603-016-1013-1.

Griffith, A.A. (1920), "The phenomenon of rupture and flow in solids", *Philos. Trans. A.*, **221**, 163-198.

Hadi, H., Alireza, K. and Mohammad, F.M. (2015), "Fracture analyses of different pre-holed concrete specimens under compression", *Acta Mech. Sin.*, **31**(6), 855-870. https://doi.org/10.1007/s10409-015-0436-3.

Hazzard, J.F., Young, R.P. and Maxwell, S.C. (2000), "Micromechanical modeling of cracking and failure in brittle rocks", *J. Geophys. Res. Solid Earth*, **105**(B7),16683-16697. https://doi.org/10.1029/2000JB900085.

Hoek, E. and Brown, E.T. (1980), *Underground Excavations in Rock*, Institute Mining and Metallurgy, CRC Press, London,

U.K.
Irwin, G.R. (1957), "Analysis of stresses and strains near the end of a crack traversing a plate", *J. Appl. Mech*., **24**, 361-364.
Itasca Consulting Group Inc. (2014), PFC (particle flow code), version 5.0, ICG, Minneapolis, Minnesota, U.S.A. http://www.itascacg.com/software/pfc.
Janeiro, R.P. and Einstein, H.H. (2010), "Experimental study of the cracking behavior of specimens containing inclusions (under uniaxial compression)", *Int. J. Fract Eng*., **164**(1), 83-102. https://doi.org/10.1007/s10704-010-9457-x.
Katcoff, C.Z. and Graham-Brady, L.L. (2014), "Modeling dynamic brittle behavior of materials with circular flaws or pores", *Int. J. Solids Struct*., **51**(3-4), 754-766. https://doi.org/10.1016/j.ijsolstr.2013.11.004.
Komurlu, E., Kesimal, A. and Demir, S. (2016), "Experimental and numerical analyses on determination of indirect (splitting) tensile strength of cemented paste backfill materials under different loading apparatus", *Geomech. Eng*., **10**(6), 775-791. https://doi.org/10.12989/gae.2016.10.6.775.
Lee, H. and Jeon, S. (2011), "An experimental and numerical study of fracture coalescence in pre-cracked specimens under uniaxial compression", *Int. J. Solids Struct*., **48**(6), 979-999. https://doi.org/10.1016/j.ijsolstr.2010.12.001.
Lee, J. and Hong, J.W. (2018), "Crack initiation and fragmentation processes in pre-cracked rock-like materials", *Geomech. Eng*., **15**(5), 1047-1059. https://doi.org/10.12989/gae.2018.15.5.1047.
Lisjak, A. and Grasselli, G. (2014), "A review of discrete modeling techniques for fracturing processes in discontinuous rock mass", *J. Rock Mech. Geotech. Eng*., **6**(4), 301-314. https://doi.org/10.1016/j.jrmge.2013.12.007.
Maji, A.K. and Shah, S.P. (1989), "Application of acoustic emission and laser holography to study microfracture in concrete", *Acids Spec. Publ*., **112**, 83-110.
Miao, S.T., Pan, P.Z., Wu, Z.H. and Zhao, S.K. (2018), "Fracture analysis of sandstone with a single filled flaw under uniaxial compression", *Eng. Fract. Mech*., **204**, 19-343. https://doi.org/10.1016/j.engfracmech.2018.10.009.
Morgan, S.P. and Einstein, H.H. (2017), "Cracking processes affected by bedding planes in Opalinus shale with flaw pairs", *Eng. Fract. Mech*., **176**, 213-234. https://doi.org/10.1016/j.engfracmech.2017.03.003.
Sammis, C.G. and Ashby, M.F. (1986), "The failure of brittle porous solids under compressive stress states", *Acta Metall*., **34**(3), 511-526. https://doi.org/10.1016/0001-6160(86)90087-8.
Tasdemir, M.A., Maji, A.K. andShah, S.P. (1989), "Crack propagation in concrete under compression", *J. Eng. Mech*., **116**(5), 1058-1076. https://doi.org/10.1061/(asce)0733-9399(1990)116:5(1058).
Wang, X., Yuan, W., Yan, Y. and Zhang, X. (2020), "Scale effect of mechanical properties of jointed rock mass: A numerical study based on particle flow code", *Geomech. Eng*., **21**(3), 259-268. https://doi.org/10.12989/gae.2020.21.3.259.
Wen, Z.J., Wang, X. Chen, L.J., Lin, G. and Zhang, H.L. (2017), "Size effect on acoustic emission characteristics of coal-rock damage evolution", *Adv. Mater. Sci. Eng*., 3472485. https://doi.org/10.1155/2017/3472485
Wong, R.H. and Lin, P. (2015), "Numerical study of stress distribution and crack coalescence mechanisms of a solid containing multiple holes", *Int. J. Rock Mech. Min. Sci*., **79**, 41-54. https://doi.org/10.1016/j.ijrmms.2015.08.003.
Wu, M. and Wang, J. (2020), "A DEM investigation on crushing of sand particles containing intrinsic flaws", *Soils Found*., **60**(2), 567-572. https://doi.org/10.1016/j.sandf.2020.03.007.
Wu, M., Wang, J., Russell, A. and Cheng, Z. (2020), "DEM modelling of mini-triaxial test based on one-to-one mapping of sand particles", *Géotechnique*, 1-14. https://doi.org/10.1680/jgeot.19.P.212.
Wu, N., Liang, Z.Z., Zhou, J.R. and Zhang, L.Z. (2020), "Energy evolution characteristics of coal specimens with preformed holes under uniaxial compression", *Geomech. Eng*., **20**(1), 55-66. https://doi.org/10.12989/gae.2020.20.1.055.
Zaitsev, Y.B. and Wittmann, F.H. (1981), "Simulation of crack propagation and failure of concrete", *Mater. Struct*., **83**(14), 357-365. https://doi.org/10.1007/BF02478729.
Zhao, J.H., Zhang, X.G., Jiang, N., Yin, L.M. and Guo, W.J. (2020), "Porosity zoning characteristics of fault floor under fluid-solid coupling", *B. Eng. Geol. Environ*., **79**(5), 2529-2541. https://doi.org/10.1007/s10064-019-01701-0.
Zhu, Q.Q., Li, D.Y., Han, Z.Y., Li, X.B and Zhou, Z.L. (2019), "Mechanical properties and fracture evolution of sandstone specimens containing different inclusions under uniaxial compression", *Int. J. Rock Mech. Min. Sci*., **115**, 33-47. https://doi.org/10.1016/j.ijrmms.2019.01.010.

GC